Arch Appl Mech (2005) 74: 637–647
DOI 10.1007/s00419-005-0385-6

ORIGINAL

M. A. Savi · A. Paiva

Describing internal subloops due to incomplete phase transformations in shape memory alloys

Received: 29 December 2004 / Accepted: 11 March 2005 / Published online: 17 June 2005

Abstract The hysteretic response of shape memory alloys (SMAs) is one of their essential characteristics and is related to the martensitic phase transformation. The hysteresis loop may be observed either in stress–strain or strain–temperature curves. In brief, it is possible to say that the major (or external) hysteresis loop can be defined as the envelope of all minor (or internal) hysteresis loops, usually denoted as subloops. The macroscopic description of the SMA hysteresis loops, together with their subloops due to incomplete phase transformations, is an important aspect in the phenomenological description of the thermomechanical behavior of SMAs, being of great interest in technological applications. This contribution exploits the description of these internal subloops and employs a constitutive model previously proposed by [1,20,25]. Numerical investigations of the phenomenon are carried out to show the capability of this model to describe these inner subloops. Comparisons between numerical and experimental results show that they are in close agreement. Moreover, numerical simulations are carried out to elucidate different aspects of this hysteretic behavior.

Keywords Shape memory alloys · Constitutive model · Hysteresis · Subloops · Numerical simulation

1 Introduction

Shape memory alloys (SMAs) are metallic compounds that are attracting much technological interest due to their remarkable properties, motivating different applications in several fields of sciences and engineering. Due to their functional properties, SMAs have obtained great success in biomedical applications, increasing both the possibility and the performance of minimal-invasion surgeries. The biocompatibility of these alloys is one of the important points related to biomedical applications [13]. Non-medical applications are also numerous in different areas, including robotics, aerospace, structural control as well as everyday applications. For a detailed description of SMAs applications, see the references [3,6,7,10,11,13,14,19,24,32,33].

Shape memory alloys display complex thermomechanical behavior related to different physical processes, which makes their description unusually difficult. The hysteretic response of SMAs is one of their essential characteristics and is related to the martensitic phase transformation. The hysteresis loop is mainly caused by frictional effects associated with the movement of austenite–martensite interfaces and martensite–martensite interfaces with different crystallographic orientations. Basically, the hysteresis loop may be observed either in stress–strain curves or strain–temperature curves. In brief, it is possible to say that the major (or external) hysteresis loop can be defined as the envelope of all minor (or internal) hysteresis loops, usually denoted as subloops [2,5,16].

M. A. Savi · A. Paiva (✉)
Universidade Federal do Rio de Janeiro, COPPE – Department of Mechanical Engineering 21.945.970 – Rio de Janeiro - RJ - Brazil, P.O. Box: 68.503
E-mail: savi@ufrj.br, paiva@lavi.coppe.ufrj.br

The macroscopic description of the SMA hysteresis loops, together with their subloops due to incomplete phase transformations, is an important aspect in the phenomenological description of the thermomechanical behavior of SMAs, being of great interest in technological applications.

The literature reports many efforts related to the analysis of SMA hysteresis loops. Both theoretically and experimental points of view are considered. Muller and Xu [15] present a study on the pseudoelastic behavior of SMAs, exploiting the description of inner loops. The model is based on polynomial Landau–Devonshire theory and considers that states inside the hysteresis loop are metastable. The cited reference compares results obtained with the proposed model with those obtained by experimental tests. In general, it is possible to say that the model is able to describe subloops related to pseudoelasticity. Ortin [16] revisits the description of SMA subloops in pseudoelasticity by considering the Preisach model. Again, the proposed model captures the general behavior of internal subloops related to pseudoelasticity. Tanaka et al. [29] analyze subloops related to either the stress–strain or strain–temperature curves. The proposed model is based on the model with assumed phase-transformation kinetics previously presented by Tanaka and Nagaki [27]. After that, other models with assumed phase-transformation kinetics are employed to describe the thermomechanical behavior of internal subloops. Brinson and Huang (1996) present results that show the capability of these models to describe subloops. Different aspects of subloops are also treated in Tanaka et al. [30], where a discussion about plateaus in the stress–strain hysteresis in SMAs is carried out. Bo and Lagoudas [4] present a phenomenological model using information based on the Preisach model to account for minor hysteresis loops correctly. Comparisons between the cited model predictions and the experimental results show that it can describe the minor loop hysteresis related to the strain–temperature response of SMAs.

This contribution exploits the description of the internal subloops due to incomplete phase transformations related to the thermomechanical response of SMAs by employing a constitutive model previously proposed by Savi et al. [25], Baêta-Neves et al. [1] and Paiva et al. [20]. A numerical investigation of the phenomenon is carried out that shows the capability of this model to describe these subloops. Comparisons between numerical and experimental results show that they are in close agreement. Moreover, numerical simulations are carried out that elucidate different aspects of this hysteretic behavior in either the stress–strain or strain–temperature responses.

2 Constitutive model

There are various ways to describe the thermomechanical behavior of SMAs (Paiva and Savi 2004). Here, a constitutive model that is built upon Fremond's [8,9] model and previously presented in various references [1, 20,25] is employed. This model considers different material properties and four macroscopic phases for the description of the SMA behavior. The model also considers plastic strains and plastic-phase transformation coupling, which enables the description of the two-way shape memory effect. Moreover, tensile–compressive asymmetry is taken into account.

The model formulation considers, besides elastic strain, ε_e, and temperature, T, four more state variables associated with the volumetric fraction of each phase: β_1 is associated with tensile detwinned martensite, β_2 is related to compressive detwinned martensite, β_3 represents austenite and β_4 corresponds to twinned martensite. A free-energy potential is proposed considering each isolated phase. After this definition, a free energy of the mixture can be written by weighting each energy function with its volumetric fraction. Since $\beta_1+\beta_2+\beta_3+\beta_4=1$, it is possible to rewrite the free energy of the mixture as a function of three volumetric fractions: β_n $(n=1,2,3)$. After this, an additive decomposition is assumed where the elastic strain may be written as: $\varepsilon_e=\varepsilon-\varepsilon_p-\alpha_h(\beta_1-\beta_2)$. Parameter α_h is introduced to define the horizontal width of the stress–strain hysteresis loop. Finally, a pseudo-potential for dissipation is defined as a function of the rates $\dot{\varepsilon}$, $\dot{T}$ and $\dot{\beta}_n$. By employing the standard generalized material approach [12], it is possible to obtain a complete set of constitutive equations that describes the thermomechanical behavior of SMAs presented below:

$$\sigma = E\left(\varepsilon-\varepsilon_p+\alpha_h^{C}\beta_2-\alpha_h^{\mathrm{T}}\beta_1\right)+\alpha^{C}\beta_2-\alpha^{\mathrm{T}}\beta_1-\Omega\,(T-T_0) \tag{1}$$

$$\begin{aligned}\dot{\beta}_1 = \frac{1}{\eta_1}\Big\{&\alpha^{\mathrm{T}}\left(\dot{\varepsilon}-\dot{\varepsilon}_p\right)+\Lambda_1+\beta_2\left(\alpha_h^{C}\alpha^{\mathrm{T}}+\alpha_h^{\mathrm{T}}\alpha^{C}+E\alpha_h^{\mathrm{T}}\alpha_h^{C}\right)\\ &-\beta_1\left(2\,\alpha_h^{\mathrm{T}}\alpha^{\mathrm{T}}+E\,\alpha_h^{\mathrm{T}^2}\right)+\alpha_h^{\mathrm{T}}\left[E\,\left(\varepsilon-\varepsilon_p\right)-\Omega\,(T-T_0)\right]\\ &-\eta_{ci}\,K\gamma-\eta_{ck}\frac{\mu}{H}-\partial_1 J_\pi\Big\}+\partial_1 J_\chi\end{aligned} \tag{2}$$

$$\dot{\beta}_2 = \frac{1}{\eta_2}\left\{-\alpha^C\left(\varepsilon-\varepsilon_p\right)+\Lambda_2+\beta_1\left(\alpha_h^{\mathrm{T}}\alpha^C+\alpha_h^C\alpha^{\mathrm{T}}+E\alpha_h^C\alpha_h^{\mathrm{T}}\right)\right.$$
$$-\beta_2\left(2\,\alpha_h^C\alpha^C+E\,\alpha_h^{C^2}\right)-\alpha_h^C\left[E\,\left(\varepsilon-\varepsilon_p\right)-\Omega\,(T-T_0)\right]$$
$$\left.-\eta_{ci}\,K\gamma-\eta_{ck}\frac{\mu}{H}-\partial_2 J_\pi\right\}+\partial_2 J_\chi \tag{3}$$

$$\dot{\beta}_3 = \frac{1}{\eta_3}\left\{-\frac{1}{2}\,(E_A-E_M)\left(\varepsilon-\varepsilon_p+\alpha_h^C\beta_2-\alpha_h^{\mathrm{T}}\beta_1\right)^2+\Lambda_3\right.$$
$$+(\Omega_A-\Omega_M)\,(T-T_0)\left(\varepsilon-\varepsilon_p+\alpha_h^C\beta_2-\alpha_h^{\mathrm{T}}\beta_1\right)$$
$$-\frac{1}{2}\,(K_A-K_M)\,\gamma^2-\left(\frac{1}{2\,H_A}-\frac{1}{2\,H_M}\right)\mu^2$$
$$\left.+\eta_{ci}\,K\gamma+\eta_{ck}\frac{\mu}{H}-\partial_3 J_\pi\right\}+\partial_3 J_\chi \tag{4}$$

$$\dot{\varepsilon}_p = \lambda\ \mathrm{sign}\ (\sigma-\mu) \tag{5}$$

$$\dot{\gamma} = \left|\,\dot{\varepsilon}_p,\right| + \eta_{ci}\left(\dot{\beta}_1+\dot{\beta}_2-\dot{\beta}_3\right) \tag{6}$$

$$\dot{\mu} = H\,\dot{\varepsilon}_p+\eta_{ck}\left(\dot{\beta}_1+\dot{\beta}_2-\dot{\beta}_3\right) \tag{7}$$

where $E = E_M+\beta_3\,(E_A-E_M)$ is the elastic modulus while $\Omega = \Omega_M+\beta_3\,(\Omega_A-\Omega_M)$ is related to the thermal expansion coefficient. Moreover, $K = K_M-\beta_3(K_M-K_A)$ is the plastic modulus and $\frac{1}{H} = \frac{1}{H_M}-\beta_3\left(\frac{1}{H_M}-\frac{1}{H_A}\right)$ is the kinematic hardening modulus. Notice that subscript A refers to austenitic phase, while M refers to martensite. Besides, assuming that the superscript T refers to tensile while C is related to compressive properties, it is possible to present the following parameters: α and α_h are parameters respectively associated with the vertical and horizontal sizes of the hysteresis loop. Moreover, the parameters $\Lambda_1 = \Lambda_1(T)$, $\Lambda_2 = \Lambda_2(T)$ and $\Lambda_3 = \Lambda_3(T)$ are associated with phase-transformation stress levels.

The terms $\partial_n J_\pi$ $(n = 1, 2, 3)$ are sub-differentials of the indicator function J_π with respect to β_n (Rockafellar, 1970). The indicator function J_π $(\beta_1, \beta_2, \beta_3)$ is related to the following convex set π, which provides the internal constraints related to the phases' coexistence.

$$\pi = \{\beta_n \in \Re\ |\, 0 \le \beta_n \le 1; \quad \beta_1+\beta_2+\beta_3 \le 1\}\ . \tag{8}$$

With respect to the evolution equations of the volumetric fractions, η_1, η_2 and η_3 represent the internal dissipation related to phase transformations. Moreover $\partial_n J_\chi$ $(n = 1, 2, 3)$ are sub-differentials of the indicator function J_χ with respect to $\dot{\beta}_n$ (Rockafellar 1970). This indicator function related to the convex set χ, establishes conditions for the correct description of internal subloops due to incomplete phase transformations and also eliminate the phase transformations $M+ \to M$ or $M- \to M$. Hence, the convex set χ may be written as follows for a mechanical loading history with $\dot{\sigma} \neq 0$:

$$\chi = \left\{ \dot{\beta}_n \in \Re \;\middle|\; \begin{array}{lll} \dot{\varepsilon}\ \dot{\beta}_1 \ge 0; & \dot{\varepsilon}\ \dot{\beta}_3 \le 0 & \text{if } \varepsilon_0 > 0 \\ \dot{\varepsilon}\ \dot{\beta}_2 \le 0; & \dot{\varepsilon}\ \dot{\beta}_3 \ge 0 & \text{if } \varepsilon_0 < 0 \end{array} \right\}, \tag{9}$$

where

$$\varepsilon_0 = \varepsilon-\frac{\Omega}{E}(T-T_0) \tag{10}$$

On the other hand, when $\dot{\sigma} = 0$, the convex set χ is expressed by

$$\chi = \left\{ \dot{\beta}_n \in \Re \;\middle|\; \begin{array}{l} \dot{T}\ \dot{\beta}_1 \begin{cases} < 0 & \text{if } \dot{T} > 0\,, \sigma < \sigma_{\mathrm{M}}^{\mathrm{crit}} \text{ and } \beta_1^s \neq 0 \\ = 0 & \text{otherwise} \end{cases} \\ \\ \dot{T}\ \dot{\beta}_2 \begin{cases} < 0 & \text{if } \dot{T} > 0\,, \sigma < \sigma_{\mathrm{M}}^{\mathrm{crit}} \text{ and } \beta_2^s \neq 0 \\ = 0 & \text{otherwise} \end{cases} \\ \dot{T}\ \dot{\beta}_3 \ge 0 \\ -\dot{\beta}_1^2-\dot{\beta}_1\dot{\beta}_3 = 0 \quad \text{or} \quad -\dot{\beta}_2^2-\dot{\beta}_2\,\beta_3 = 0 \end{array} \right\} \tag{11}$$

Table 1 Model parameters for a Ni–Ti SMA [15]

E_A (GPa)	E_M (GPa)	Ω_A (MPa/K)	Ω_M(MPa/K)	α^T (MPa)
6.5	4.65	0.74	0.17	1.95
L_0^{T} (MPa)	L^{T} (MPa)	L_0^A (MPa)	L^A (MPa)	$\varepsilon_R^{\mathrm{T}}$
36.83	230	20	180	0.052
η_1^L (kPa.s)	η_1^U (MPa.s)	η_3^L (MPa.s)	η_3^U (MPa.s)	
89.6	77.5	89	77	
T_M (K)	T_0 (K)			
263	378			

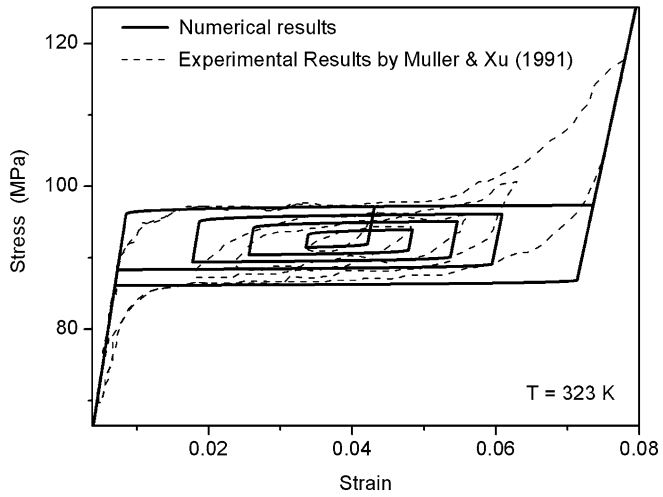

Fig. 1 Comparison between numerical and experimental results by [15] for pseudoelastic subloops

where β_1^s and β_2^s are the values of β_1 and β_2, respectively, when the phase transformation begins to take place. Moreover, σ_M^{crit}, which actually has different values for tensile or compressive behaviors ($\sigma_M^{T\mathrm{crit}}and\sigma_M^{C\mathrm{crit}}$), are the critical stress values for $M \rightarrow M+$ and $M \rightarrow M$ phase transformations.

For the definition of the parameters, it is important to evaluate the functions Λ_1, Λ_2 and Λ_3, which are temperature dependent as follows:

$$\Lambda_1 = -L_0^{\mathrm{T}} + \frac{L^{\mathrm{T}}}{T_M}(T - T_M)\,, \tag{12}$$

$$\Lambda_2 = -L_0^{C} + \frac{L^{C}}{T_M}(T - T_M)\,, \tag{13}$$

$$\Lambda_3 = -L_0^{A} + \frac{L^{A}}{T_M}(T - T_M)\,. \tag{14}$$

Here, T_M is the temperature below which the martensitic phase becomes stable. Besides, L_0^{T}, L^{T}, L_0^C, L^C, L_0^A and L^A are parameters related to the critical stress for phase transformation, remembering that the indexes T refer to tensile, C to compression and A to austenite.

The definition of these functions establishes the phase-transformation critical stress for each phase. Actually, the definition of critical stress is essential to evaluate the convex set χ when $\dot{\sigma} = 0$. It may be obtained from Eqs. (1) and (2), considering $\dot{\beta}_1 = \beta_1 = \beta_2 = \beta_3 = 0$. Therefore, the following expression is obtained for tensile behavior

$$\sigma_M^{\mathrm{Tcrit}} = \frac{E_M}{\alpha^{\mathrm{T}} + E_M \alpha_h^{\mathrm{T}}}\left[L_0^{\mathrm{T}} - \frac{L^{\mathrm{T}}(T - T_M)}{T_M} + \alpha_h^{\mathrm{T}}\Omega_M(T - T_0) + \eta_{ci} K_M \gamma + \eta_{ck}\frac{\mu}{H_M}\right] - \Omega_M(T - T_0)\,. \tag{15}$$

Table 2 Model parameters for a Cu–Zn–Al–Mn SMA (Sittner et al. 1995)

E_A (GPa)	E_M (GPa)	Ω_A (MPa/K)	Ω_M(MPa/K)	α^T (MPa)
35	27.1	0.74	0.17	0.5
L_0^{T} (MPa)	L^{T} (MPa)	L_0^A (MPa)	L^A (MPa)	$\varepsilon_R^{\mathrm{T}}$
36.83	169	20	109	0.0074
η_1^L (MPa.s)	η_1^U (MPa.s)	η_3^L (MPa.s)	η_3^U (MPa.s)	
327	261	357	209	
T_M (K)	T_0 (K)			
225	285			

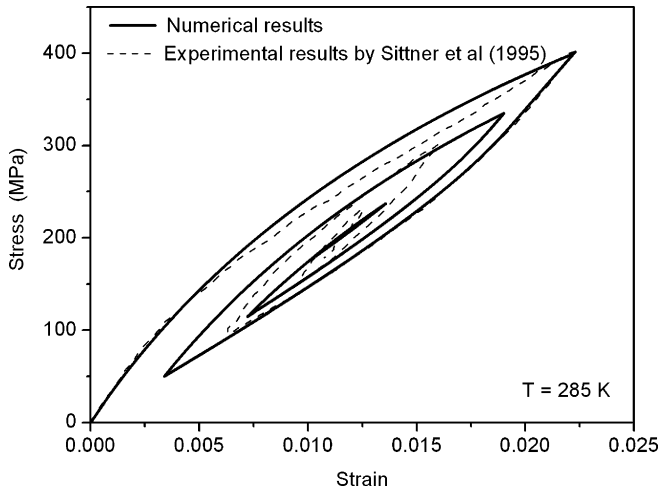

Fig. 2 Comparison between numerical and experimental results by [26] for pseudoelastic subloops

Another important characteristic of the model is that there is a critical temperature, T_C, below which there is no change in the stress–strain hysteresis loop position. This temperature limits the variation of the transformation critical stress and can be determined by again considering Eqs. (1) and (2), assuming that $\dot{\beta}_1 = \beta_2 = \beta_3 = 0$; $\beta_1 = 1$;$\varepsilon = \varepsilon_R^{\mathrm{T}}$; $\varepsilon_p = 0$; $T = T_C^{\mathrm{T}}$. Therefore, the following parameters are defined for tensile behavior,

$$\begin{aligned} \alpha_h^{\mathrm{T}} &= \varepsilon_R^{\mathrm{T}} - \frac{\alpha^{\mathrm{T}}}{E_M} - \frac{\Omega_M}{E_M}\left(T_C^{\mathrm{T}} - T_0\right) \\ T_C^{\mathrm{T}} &= T_M \left[\frac{\left(L_0^{\mathrm{T}} + L^{\mathrm{T}}\right) E_M + \alpha^{\mathrm{T}}(\Omega_M T_0 - \alpha^{\mathrm{T}})}{L^{\mathrm{T}} E_M + \alpha^{\mathrm{T}} \Omega_M T_M} \right] \end{aligned} \tag{16}$$

As pointed out before, the first parameter is related to the horizontal size of the stress–strain hysteresis loop for tensile behavior, which is a function of the maximum residual strain ε_R^T, which is a usual parameter obtained during the experimental characterization of SMAs.

An analogous procedure considering the evolution of β_2 defines similar parameters for compressive behavior:

$$\begin{aligned} \sigma_M^{C\mathrm{crit}} = \frac{E_M}{\alpha^C + E_M \alpha_h^C} \Bigg[& -L_0^C + \frac{L^C (T - T_M)}{T_M} + \alpha_h^C \Omega_M (T - T_0) \\ & -\eta_{ci} K_M \gamma - \eta_{ck} \frac{\mu}{H_M} \Bigg] - \Omega_M (T - T_0) \end{aligned} \tag{17}$$

Table 3 Model parameters for a Ni–Ti SMA (Tobushi et al., 1991; [20])

E_A (GPa)	E_M (GPa)	Ω_A (MPa/K)	Ω_M(MPa/K)	α^T (MPa)
54	42	0.74	0.17	330
L_0^{T} (MPa)	L^{T} (MPa)	L_0^A (MPa)	L^A (MPa)	$\varepsilon_R^{\mathrm{T}}$
0.15	41.5	0.63	185	0.0555
η_1^L (MPa.tu)	η_1^U (MPa.tu)	η_3^L (MPa.tu)	η_3^U (MPa.tu)	
1	2.7	1	2.7	
T_M (K)	T_A (K)	T_0 (K)		
291.4	307.5	307		
$\sigma_Y^{A,i}$(GPa)	$\sigma_Y^{A,f}$(GPa)	σ_Y^M (GPa)	η_{ci}	η_{ck}
1.5	1.0	0.5	−0.01	−0.01
K_A (GPa)	K_M (GPa)	H_A (GPa)	H_M (GPa)	T_F (K)
1.4	0.4	4	1.1	423

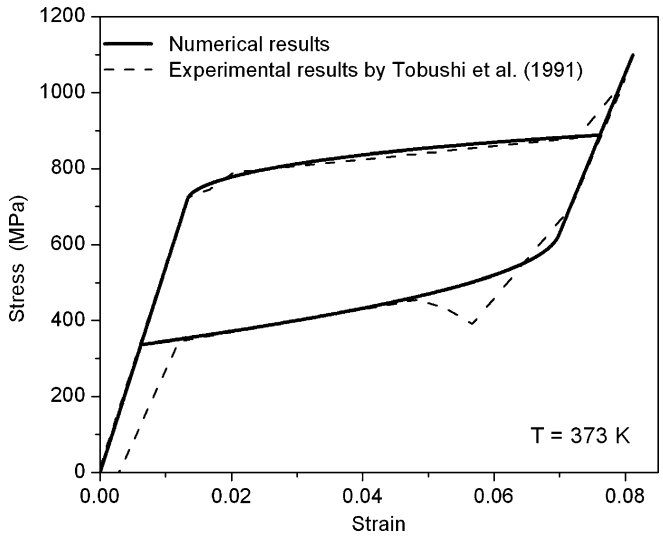

Fig. 3 Comparison between numerical and experimental results by Tobushi et al. (1991)

And also,

$$\alpha_h^C = -\varepsilon_R^C - \frac{\alpha^C}{E_M} + \frac{\Omega_M}{E_M}\left(T_C^C - T_0\right)$$
$$T_C^C = T_M\left[\frac{\left(L_0^C + L^C\right)E_M - \alpha^C(\Omega_M T_0 + \alpha^{\mathrm{T}})}{L^C E_M - \alpha^C \Omega_M T_M}\right] \tag{18}$$

Now, it should be pointed out that functions Λ_1, Λ_2 and Λ_3, do not vary for temperatures below these critical values.

To consider different characteristics of the kinetics of phase transformation for loading and unloading processes, it is possible to consider different values of the parameter η_n, which is related to internal dissipation. Therefore,

$$\begin{cases} \eta_n = \eta_n^L & \text{if } \dot{\varepsilon} > 0 \\ \eta_n = \eta_n^U & \text{if } \dot{\varepsilon} < 0 \end{cases} \tag{19}$$

where η_n^L and η_n^U are internal dissipation parameters related to variable β_n during loading or unloading process, respectively.

The yield limit σ_Y has different values for the austenitic and martensitic phases. Moreover, for very high temperatures, this value tends to decrease. Therefore, it is assumed that the yield limit has a linear variation

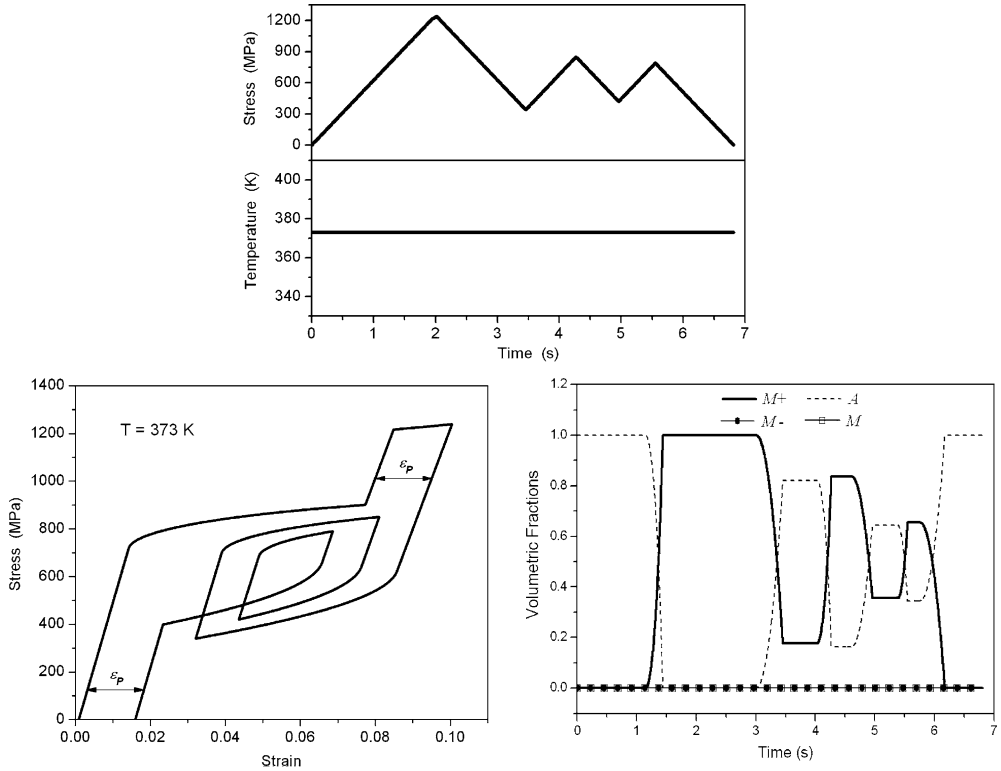

Fig. 4 Pseudelastic subloops

with T, evaluated with the following expression:

$$\begin{cases} \sigma_Y = \sigma_Y^M & \text{if } T \leq T_M \\ \sigma_Y = \frac{\sigma_Y^M (T_A - T) + \sigma_Y^{A,i} (T - T_M)}{T_A - T_M} & \text{if } T_M < T \leq T_A \\ \sigma_Y = \frac{\sigma_Y^{A,i} (T_F - T) + \sigma_Y^{A,f} (T - T_A)}{T_F - T_A} & \text{if } T_A < T \leq T_F \,, \end{cases} \tag{20}$$

where T_F is a reference temperature related to high values of temperature and T_A is the temperature above which austenite is the only stable phase.

The solution of the constitutive equations employs an implicit Euler method together with the operator split technique (Ortiz et al. 1983). For β_n $(n = 1, 2, 3)$ calculation, the evolution equations are solved in a decoupled way. At first, the equations (except for the sub-differentials) are solved using an iterative implicit Euler method. If the estimated results obtained for β_n does not fit the imposed constraints, an orthogonal projection algorithm pulls their value to the nearest point on the domain's surface ([20,21]).

3 Model verification

This section presents verification of the capability of the proposed model to describe the general thermomechanical behavior related to subloops. With this aim, comparisons between the results predicted by the proposed model and experimental data reported in literature are of concern. At first, we focus on pseudoelasticity, considering experimental tests presented in Muller and Xu [15] as a reference. The pseudoelastic response describes tensile tests on Ni–Ti wires subjected to isothermal nonproportional mechanical loading that results in incomplete phase transformations. The model parameters adjusted for this simulation are presented in Table 1. Since plastic and compressive behaviors are not considered, the material parameters related to these phenomena are omitted. Figure 1 presents a comparison between numerical and experimental results, showing good agreements.

Figure 2 shows a different test related to nonproportional loadings. Basically, the SMA specimen is subjected to a different loading process, resulting in the presented results. Again, we focus on pseudoelasticity,

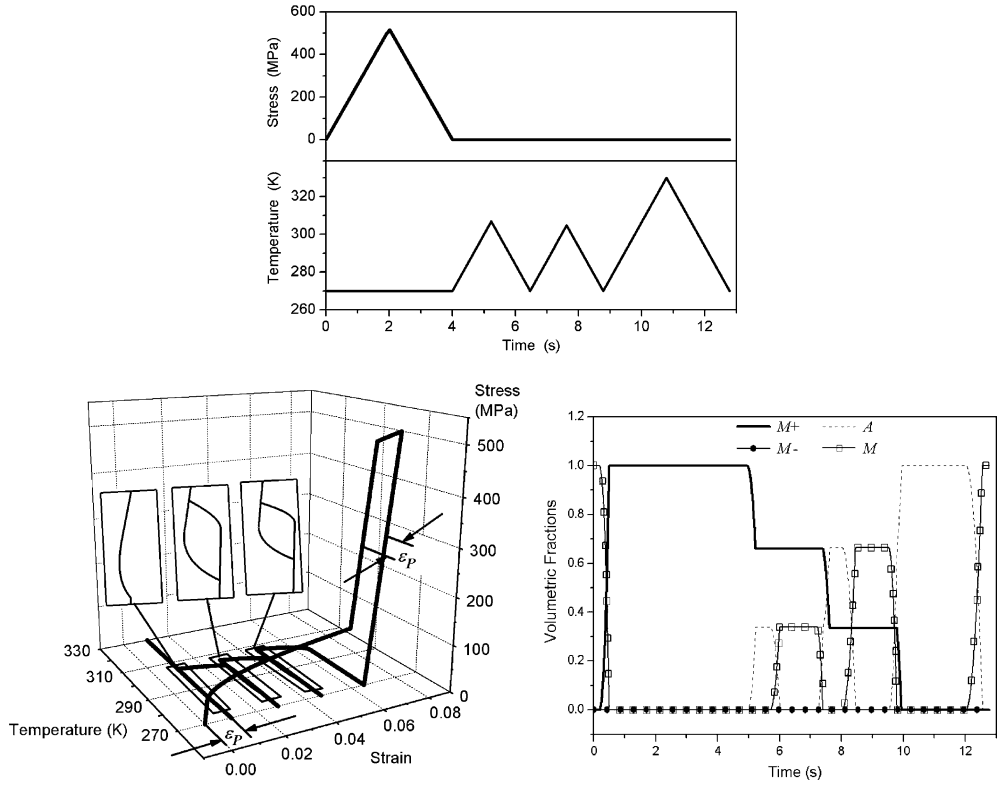

Fig. 5 Shape memory effect subloops

considering experimental tests presented in Sittner et al. [26] as a reference. The pseudoelastic response describes tensile tests on Cu–Zn–Al–Mn polycrystalline SMA at 285 K. The model parameters adjusted for this simulation are presented in Table 2. Notice that numerical simulation captures the general behavior of this thermomechanical response.

4 Numerical simulations

Numerical simulations are now carried out considering various thermomechanical loadings to show the potential of the discussed model to describe SMA behavior, especially related to inner subloops due to incomplete phase transformations. The calibration of the proposed model is done by comparing numerical simulation with experimental data presented by Tobushi et al. (1991) that describes tensile tests on Ni–Ti wires. A temperature $T = 373$ K is used to calibrate the model parameters to reproduce the experimental data. Table 3 presents the adjusted parameters and also parameters related to the plastic behavior ([20]). Figure 3 shows both numerical and experimental data showing good agreements. For the sake of simplicity, one uses a time unit (tu) that is representative of the loading rate.

At this point, considering the adjusted parameters, numerical simulations are performed to explore different aspects of SMAs' behavior, especially those related to internal subloops. At first, pseudoelastic behavior is considered using the isothermal loading process shown in Fig. 4. Initially, the loading process induces the phase transformation $A \rightarrow M+$, and continues to be applied, completing this transformation and reaching the yield surface. During the unloading process, the reverse transformation ($M+ \rightarrow A$) begins to take place; however, during this transformation, the specimen is reloaded before the phase transformation is completed. This new loading process induces a linear response before the phase transformation $A \rightarrow M+$ begins to occur. This response is related to an internal subloop. Similar cycles of loading–unloading process continue to be applied, imposing incomplete phase transformations. This process induces other internal subloops in the stress–strain curves as shown in Fig. 4. Figure 4 also shows the phase volumetric fractions clearly presenting the evolution of incomplete phase transformation.

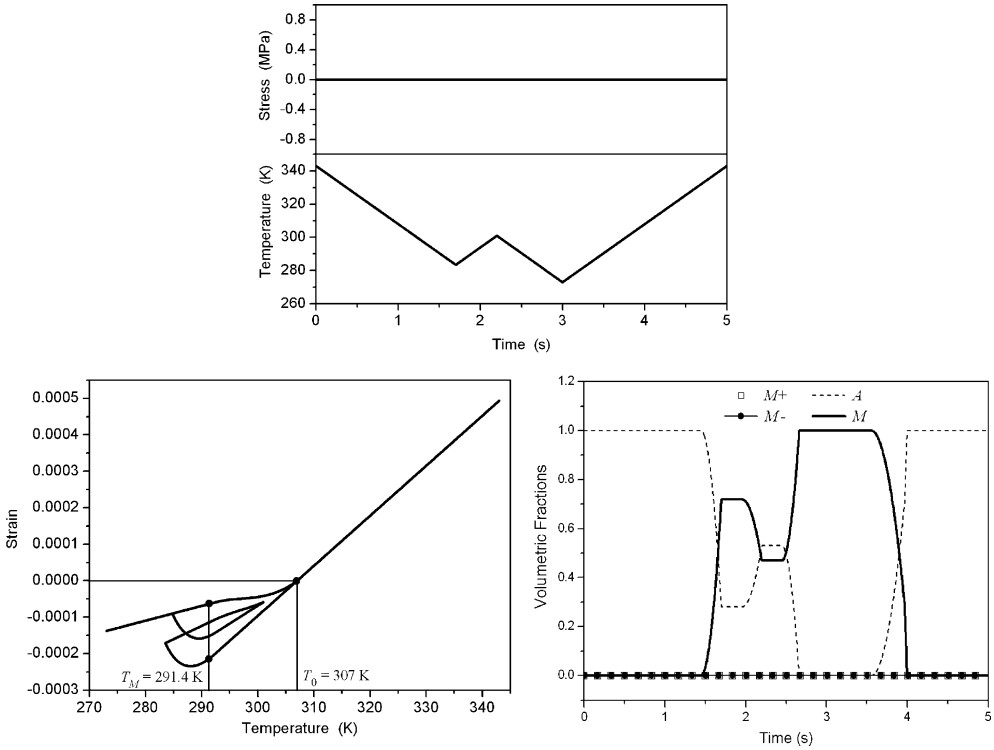

Fig. 6 Thermal subloops

Now, shape memory effect is considered on Fig. 5, where the phase transformations are related to different phases. Initially, a constant temperature $T = 270\,\mathrm{K}$ ($T < T_M$) is considered, where twinned martensite M is a stable phase. After a mechanical loading is applied, the specimen experiences the phase transformation from twinned martensite to detwinned martensite ($M \rightarrow M+$). In this stage, the loading process continues to be applied and the yield surface is reached. After that, the unloading process promotes elastic unloading, which reveals the presence of residual strain. After this mechanical loading, a nonproportional thermal loading is applied, inducing incomplete phase transformation. The heating related to the first cycle causes the transformation of part of martensitic variant $M+$ to austenite, A. The subsequent cooling of this first cycle tends to convert the austenite A to twinned martensite, M, while detwinned martensite ($M+$) remains constant. The second cycle continues to promote the transformation $M+ \rightarrow A$ during heating, and $A \rightarrow M$ during cooling. Finally, the last thermal cycle promotes the complete transformation $M+ \rightarrow A$ during heating, which recovers the residual stress associated to phase transformation but not that related to the plastification process and, during cooling, the transformation $A \rightarrow M$ takes place. Phase volumetric fractions evolution shows the sequence of the phase transformations described before.

At this point, internal subloops related to phase transformation due to temperature variation at a stress-free state are considered (Fig. 6). Initially, the specimen is at a high temperature where austenite is stable. The decrease in temperature causes the phase transformation from austenite to martensite ($A \rightarrow M$). During this phase transformation, a heat process is imposed and the specimen experiences a linear dilatation before the reverse phase transformation ($M \rightarrow A$) associated with the internal subloop starts. After that, a cooling process is imposed causing the specimen contraction. By increasing the temperature, phase transformation $A \rightarrow M$ begins to take place until it finishes.

The stress-induced martensite training (SIM training) related to the two-way shape memory effect (Fig. 7). Initially, 20 cycles of an isothermal mechanical process ($T = 373\,\mathrm{K}$), with increasing maximum values, is considered, causing plastic strains. After this mechanical process, thermal load is applied while maintaining a constant value of mechanical load ($\sigma = 100\,\mathrm{MPa}$). Figure 7 shows the stress–strain curve related to this thermomechanical loading process. Notice the growth of plastic strains during each load cycle. On finishing this process, the SMA displays phase transformation $A \rightarrow M+$ during cooling and $M+ \rightarrow A$ during heating. This behavior is related to the two-way shape memory effect that allows one to associate each phase with a different form. Here, after SIM training is complete, the specimen is subjected to a nonproportional thermal loading

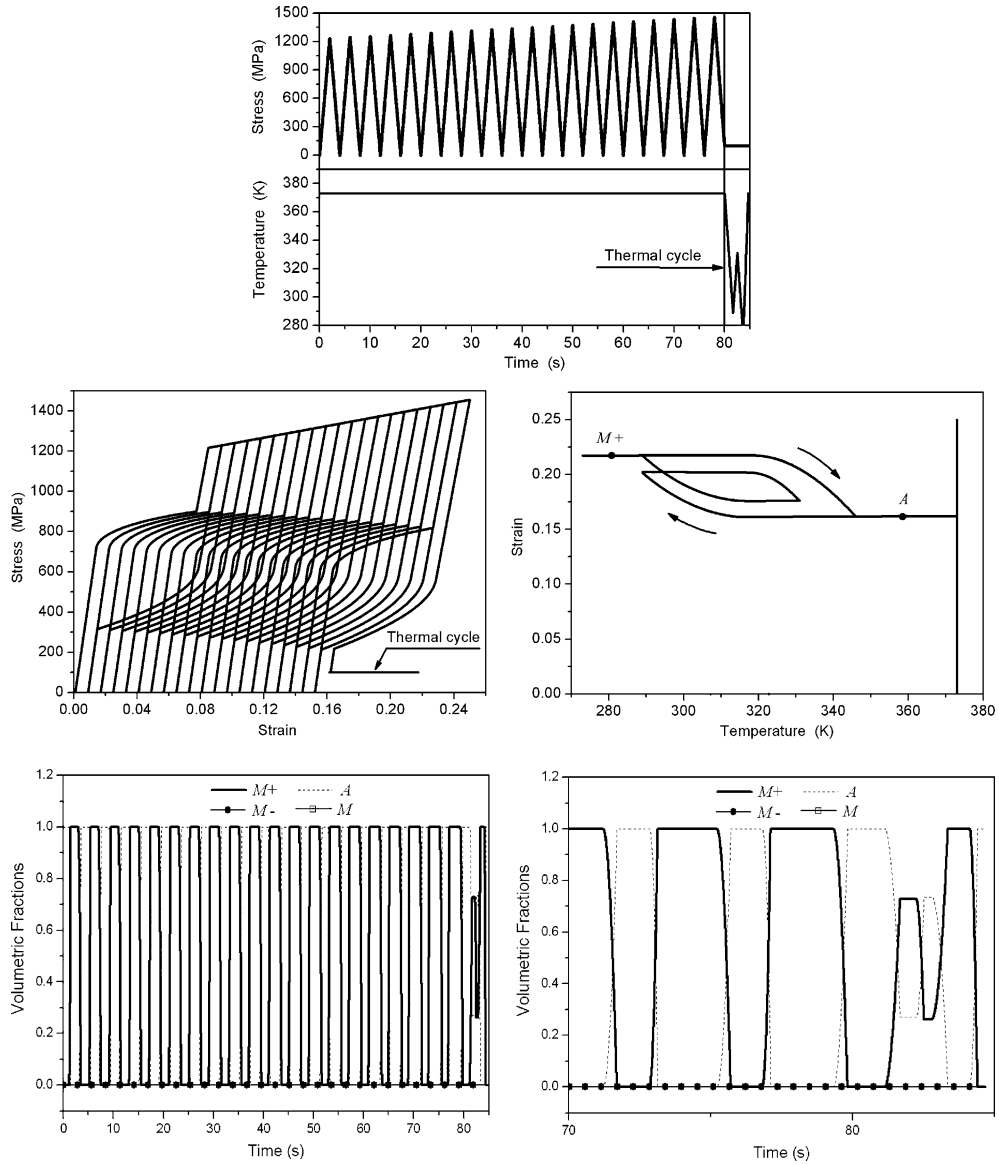

Fig. 7 Two-way subloops

process which induces incomplete phase transformation. This process may be seen in the strain–temperature curve, also shown in Fig. 7. The internal subloop is analogous to that presented during a thermal loading in the stress-free state, discussed in the previous simulation. However, the phases involved in this transformation are the detwinned martensite $M+$ and the austenite A.

5 Conclusions

The present contribution discusses some features related to the description of the SMA internal subloops due to incomplete phase transformation. A constitutive model previously presented in Paiva et al. [20] is employed to describe the thermomechanical behavior of SMA. Comparisons between numerical and experimental results show the capacity of the model to capture the general behavior of inner subloops in SMAs. Moreover, a numerical investigation is carried out for different thermomechanical loadings. This investigation shows some aspects related to the inner subloops due to incomplete phase transformation. Pseudoelasticity, shape memory effect and phase transformation phenomenon due to temperature variation are evaluated. In general, the

model presented here is capable of capturing the thermomechanical behavior of SMA for a great variety of phenomena, showing interesting results relating to phase transformations.

Acknowledgements The authors acknowledge the support of the *Brazilian Research Council (CNPq)*.

References

1. Baêta-Neves, A.P., Savi, M.A., Pacheco, P.M.C.L.: On the Fremond's constitutive model for shape memory alloys. Mech Res Commun **31**(6), 677–688 (2004)
2. Benzaqui, H., Lexcellent, C., Chaillet, N., Lang, B., Bourjault, A.: Experimental study and modeling of a TiNi shape memory wire actuator. J Intell Mater Syst Struct **8**, 619–629 (1997)
3. Birman, V.: Theory and comparison of the effect of composite and shape memory alloy stiffeners on stability of composite shells and plates. Int J Mech Sci **39**(10), 1139–1149 (1997)
4. Bo, Z.H., Lagoudas, D.C.: Thermomechanical modeling of polycrystalline SMAs under cyclic loading – Part IV: modeling of minor hysteresis loops. Int J Eng Sci **37**, 1205–1249 (1999)
5. Brinson, L.C., Huang, M.S.: Simplifications and comparisons of shape memory alloy constitutive models. J Intell Mater Syst Struct **7**(1) 108–114 (1996)
6. Denoyer, K.K., Erwin, R.S., Ninneman, R.R.: Advanced smart structures flight experiments for precision spacecraft. Acta Astronaut **47**, 389–397 (2000)
7. Duerig, T.M., Pelton, A., Stöckel, D.: An overview of nitinol medical applications. Mater Sci Eng A **273–275**, 149–160 (1999)
8. Fremond, M.: Matériaux à mémoire de forme. C.R. Acad Sc Paris Tome. 304, s. II, n. 7, 239–244 (1987)
9. Fremond, M.: Shape memory alloy: a thermomechanical macroscopic theory. CISM Courses Lect **351**, 3–68 (1996)
10. Garner, L.J., Wilson, L.N., Lagoudas, D.C., Rediniotis, O.K.: Development of a shape memory alloy actuated biomimetic vehicle. Smart Mat Struct **9**(5), 673–683 (2001)
11. Lagoudas, D.C., Rediniotis, O.K., Khan, M.M.: Applications of shape memory alloys to bioengineering and biomedical technology. In: Proceeding of 4th international workshop on mathematical methods in scattering theory and biomedical technology, Perdika, Greece, (1999)
12. Lemaitre, J., Chaboche, J.-L.: Mech Solid Mat. Cambridge University Press, Cambridge (1990)
13. Machado, L.G., Savi, M.A.: Medical applications of shape memory alloys. Braz J Med Biol Res **36**(6), 683–691 (2003)
14. Machado, L.G., Savi, M.A.: Odontological applications of shape memory alloys (in portuguese). Rev Brasileira de Odontol **59**(5), 302–306 (2002)
15. Muller, I., Xu, H.: On the pseudo-elastic hysteresis. Acta Metallurgical Mat **39**(3), 263–271 (1991)
16. Ortin, J.: Partial hysteresis cycles in shape memory alloys: experiments and modelling. J. Phys IV **1**, C4–65−C4–70 (1991)
17. Ortin, J., Delaey, L.: Hysteresis in shape memory alloys. Int J Non-Linear Mech **37**, 1275–1281 (2002)
18. Ortiz, M., Pinsky, P.M., Taylor, R.L.: Operator split methods for the numerical solution of the elastoplastic dynamic problem. Comp Meth App Mech Eng **39**, 137–157 (1983)
19. Pacheco, P.M.C.L., Savi, M.A.: Modeling and simulation of a shape memory release device for aerospace applications. Rev Engenharia e Ciências Aplicadas, (2000)
20. Paiva, A., Savi, M.A., Braga, A.M.B., Pacheco, P.M.C.L.: A constitutive model for shape memory alloys considering tensile-compressive asymmetry and plasticity. Int J Solids Struct **42** (11–12), 3439–3457 (2005)
21. Paiva, A.: Modeling of thermomechanical behavior of shape memory alloys (in portuguese). PhD Thesis, PUC-Rio, Department of Mechanical Engineering (2004)
22. Paiva, A., Savi, M.A.: An overview on constitutive models for shape memory alloys. Submitted to Math Problems in Eng (2005)
23. Rockafellar, R.T.: Convex analysis, Princeton Press (1970)
24. Rogers, C.A.: Intelligent materials. Scientific American, 1995, pp. 122–127
25. Savi, M.A., Paiva, A., Baêta-Neves, A.P., Pacheco, P.M.C.L.: Phenomenological modeling and numerical simulation of shape memory alloys: a thermo-plastic-phase transformation coupled model. J Intell Mater Syst Struct **13**(5), 261–273 (2002)
26. Sittner, P., Hara, Y., Tokuda, M.: Experimental study on the thermoelastic martensitic transformation in shape memory alloy polycrystal induced by combined external forces. Metallurgical Mater Trans A, **26A**, 2923–2935 (1995)
27. Tanaka, K., Nagaki, S.: Thermomechanical description of materials with internal variables in the process of phase transformation. Ingenieur Archiv **51**, 287–299 (1982)
28. Tanaka, K., Nishimura, F., Tobushi, H.: Phenomenological analysis on subloops in shape memory alloys due to incomplete transformations. J. Intell Mater Syst Struct **5**, 387–493 (1994)
29. Tanaka, K., Nishimura, F., Hayashi, T., Tobushi, H., Lexcellent, C.: Phenomenological analysis on subloops and cyclic behavior in shape memory alloys under mechanical and/or thermal loads. Mech Mater **19**, 281–292 (1995)
30. Tanaka, K., Nishimura, F., Matsui, M., Tobushi, H., Lin, P.-H.: Phenomenological analysis on plateaus on stress–strain hysteresis in TiNi shape memory alloy wires. Mech Mater **24**, 19–30 (1996)
31. Tobushi, H., Iwanaga, N., Tanaka, K., Hori, T., Sawads, T.: Deformation behavior of Ni-Ti shape memory alloy subjected to variable stress and temperature. Conti Mech Therm **3**, 79–93 (1991)
32. van Humbeeck, J.: Non-medical applications of shape memory alloys. Mater Sci Eng A **273–275**, 134–148 (1999)
33. Webb, G., Wilson, L., Lagoudas, D.C., Rediniotis, O.: Adaptive control of shape memory alloy actuators for underwater biomimetic applications. AIAA J **38**(2), 325–334 (2000)